Nonradiative surface plasmon assisted microscale Marangoni forces

A. Passian,[1,*] S. Zahrai,[2] A. L. Lereu,[1,†] R. H. Farahi,[1] T. L. Ferrell,[1] and T. Thundat[1]
[1]*Oak Ridge National Laboratory, Oak Ridge, Tennessee 37831, USA*
[2]*Department of Mechanics, The Royal Institute of Technology, Stockholm, Sweden*
(Received 28 February 2005; revised manuscript received 3 May 2006; published 29 June 2006)

When a liquid droplet experiences a temperature inhomogeneity along its bounding surface, a surface energy gradient is engendered, which when, in a continuous sense, exceeding a threshold, results in a convective flow dissipating the energy. If the associated temperature gradients are sustained by the interface between the liquid and a supporting substrate, the induced flow can result in the lateral motion of the droplet overcoming the viscosity and inertia. Recently, pico-liter adsorbed and applied droplets were shown experimentally to be transported, and divided by the decay of optically excited surface plasmons into phonons in a thin gold foil. The decaying events locally modify the temperature of the liquid-solid interface, establishing microscale thermal gradients of sufficient magnitude for the droplet to undergo thermocapillary flow. We present experimental evidence of such gradients resulting in local surface modification associated with the excitation of surface plasmons. We show theoretically that the observed effect is due to Marangoni forces, and computationally visualize the flow characteristics for the experimental parameters. As an application based on our results, we propose a method for an all-optical modulation of light by light mediated by the droplet oscillations. Furthermore, the results have important consequences for microfluidics, droplet actuation, and simultaneous surface plasmon resonance sensing and spectroscopy.

DOI: 10.1103/PhysRevE.73.066311 PACS number(s): 47.55.D−, 07.07.Df, 47.85.L−, 73.20.Mf

I. INTRODUCTION

The energy stored in the surface region of liquid and solid domains with its various manifestations plays a paramount role in the micrometer and submicrometer realm, where an abundance of surfaces prevails. From an electrodynamic point of view, the energy of surface modes is prescribed by the dielectric function.

In the case of liquid droplets or films at temperature T, the surface energy may also be expressed as $h=\gamma-Td\gamma/dT$, where γ [Jm^2] is the free surface energy (surface tension) [1]. In general, surface energy declines with an increase in temperature due to thermal expansion. If a droplet experiences a temperature gradient of magnitude ΔT along its surface, where the shear stress is proportional to ΔT, under proper conditions, it then attempts to move in the direction of the gradient away from the higher temperature. The surface tension forces act primarily in the direction of a normal to the liquid surface with a magnitude proportional to the local radius of curvature tending to hold the droplet spherical. The intriguing feature is, however, that a variation in the magnitude of γ may give rise to yet another force acting tangentially to the surface, driving a flow. Such convective flows are at the heart of many fascinating phenomena, such as those involved in the camphor particles dance [2] when dropped on a water surface, in Thomson's original work [3] with tears of wine, in Bénard's original work [4] with heated whale oil, and in the common observation of survivance of a coffee drop at the surface of the liquid coffee coalescing with the bulk of the liquid [5].

In the case of the surface modes of noble metals, the complex dielectric function of, for example gold (Au), supports resonance behavior for the collective motion of the conduction band electrons [6]. When excited, the quantized energy $\hbar\omega_{sp}$, surface plasmons (SPs) [7], of such motion at frequency ω_{sp}, decays through radiative and nonradiative channels due to surface roughness, impurities, and damping. The nonradiative decay of SPs of momentum κ to phonons generates a localized heat source $Q(\bar{r},t)$ proportional to the decay length L_κ in the associated nanostructures such as thin films, islands, wires, holes, etc. It is shown, in this paper, that such a source will install a thermal gradient of sufficient magnitude so as to induce a surface tension gradient along the surfaces of a nearby microdroplet causing it to experience the Marangoni effect [8]. Due to the tremendous potential of such studies for fluid manipulations at the microscale, several new works, have been emerging, including a review article [9] by Darhuber *et al.* Various approaches are currently being investigated utilizing resistive current sources [10] (and references therein), light sources [11], and optical excitation of surface plasmons [12].

Although, the gravitational effect is small due to the micrometer-thin droplets considered in this work, in general under the standard temperature and pressure (STP) conditions, Marangoni and buoyancy convections coexist. The former is the focus of this article, where the convection is driven mainly by the release of surface energy rather than of gravitational energy. Marangoni convection, is gravity independent [13], and is caused by a surface tension gradient as a result of either a density gradient (solutal) or a temperature gradient (thermocapillary) of the fluid under study. We present in the following sections, the results of our investigations of SP assisted droplet actuation and control. Section II begins with a reproduction/recapitulation of the results of SP assisted droplet transportation and division, and continues

*Electronic address: passianan@ornl.gov
†Present address: ICFO-Institut de Ciències Fotòniques, 08860 Castelldefels (Barcelona), Spain.

TABLE I. Material data for the liquids (glycerol and silicone oil) droplet, metal (gold) thin film and the dielectric (quartz) substrate.

	Glycerol	Silicone oil	Gold film	Fused silica
Length	70 μm	220 μm	1 cm	2 cm
Width	70 μm	150 μm	1 cm	2 cm
Thickness	50 μm	20 μm	34 nm	2 cm
Contact angle θ_c	50°	10°		
Index of refraction n_d	[a,c]1.451	1.405	[d]0.608+i2.12	[d]1.46
Density d	1260 kg m^{-3}	950 kg m^{-3}	[b]19300 kg m^{-3}	[b]2650 kg m^{-3}
Dynamic viscosity μ_L	1.48 Pa s^{-1} s^{-1}	0.095 Pa s^{-1} s^{-1}		
Thermal capacity	2430 J kg^{-1} K^{-1}	1800 J kg^{-1} K^{-1}	[b]127 J kg^{-1} K^{-1}	[b]738 J kg^{-1} K^{-1}
Surface tension γ	0.063 N m^{-1}	0.021 N m^{-1}		
Thermal conductivity	0.30 W m^{-1} K^{-1}	0.11 W m^{-1} K^{-1}	317 W m^{-1} K^{-1}	1.45 W m^{-1} K^{-1}
Thermal expansion	500 [10^{-6} K^{-1}]		[a]14.2 [10^{-6} K^{-1}]	[a]0.49 [10^{-6} K^{-1}]

[a]T=20°,
[b]T=25°,
[c]λ=589 nm,
[d]λ=515 nm.

with a presentation of our results of droplet differentiation and sorting, followed by experimental evidence of SP thermal modification of the surface on which the droplets reside. In Sec. III, in an attempt to establish that the Marangoni forces are the principal mechanism responsible for the droplet motion, we computationally model the observed effect and numerically simulate the results using experimental parameters. Concluding remarks are given in Sec. IV.

II. EXPERIMENTAL RESULTS AND DISCUSSIONS

The wetting properties of droplets may be quantified using the concept of contact angles θ_c. Optical microscope charge-coupled device (CCD) images of the θ_c measurements of the microdroplets used yield a contact angle of $\theta_c = 10°$ for silicon oil (SO), whereas a $\theta_c = 50°$ was measured for glycerol (Gl) droplets. The typical dimensions are in the ranges 30–250 μm length, 30–150 μm width, and 20–50 μm height, and are, along with all other material data used throughout this work, summarized in Table I. With known surface tensions for the droplet γ_L, and the gold (Au) film γ_M, the surface tension of the interface γ_{ML} may be determined utilizing the θ_c, the contact angle measurements, and $\theta_c \approx \arccos[(\gamma_M - \gamma_{ML})/\gamma_L]$.

We start our presentation by all optical microfluidic manipulation [12] of polydimethylsiloxanes (PDMS) or silicone oil (SO), and glycerol (Gl) [14] by virtue of the optical excitation of SPs in a thin gold film in the Kretschmann configuration [15]. In the context of our present work, the experimental configuration may be depicted as shown in Fig. 1, where a Au film of thickness $d=34$ nm is vacuum evaporated on a quartz (ϵ_s) 90° substrate prism. Several droplets of index of refraction n_i, surface tension γ_i, viscosity ν_i, $i = 1,2,\ldots$ may be disposed on the metallic surface, where a temperature gradient of magnitude ΔT prevails due to the decay of SPs. As shown in Fig. 1(a) the distance between the SP excitation region and the droplet is controlled by a *xy*-translation stage attached to the prism substrate allowing the study of the onset of Marangoni actuation as represented by the exaggerated cross section of the Au-droplet in Fig. 1(b).

In order to elaborate on the mechanism of the observed flow in our work, we articulate an energy transfer from the incident optical beam to the droplet as follows. To determine the total optical energy, A, absorbed in the source region, Ω_s, of diameter d_s by the process of SP excitation, one may resort to energy conservation in the Au foil $A=1-R-T$, where R, and T are the normalized reflected and transmitted power, respectively. Using p-polarized photons of wavelength $\lambda=514$ nm, in a $w_b=140$ μm wide Gaussian beam provided by an Ar^+ laser, the dielectric function of Au [16] requires a 34 nm thick smooth film for spectral optimization, when quartz with $\sqrt{\epsilon_s}=1.46$ is used as the substrate. The SP dispersion relation in the quartz-Au-air system then provides the photon incidence angle $\theta_{sp}=52°$, corresponding to SP wave-vector $\mathrm{Re}(\kappa)=2\pi\sqrt{\epsilon_s}\sin\theta_{sp}/\lambda$ for resonance excitation. It can be shown from the SP dispersion relations that replacing the air with a medium of index of refraction >1 results in a redshift of the SP energies; the essence of surface plasmon resonance (SPR) sensors. Under resonance conditions, $R=T\approx 0$. A fraction of A is, however, lost by the coupling of the nonradiative SPs to radiation due to momentum degrading roughness scattering (shown as the bright spot in Figs. 4 and 5). The source diameter d_s may be altered, for example for silver (with longer SP relaxation times) where at the same excitation wavelength λ, the decay length $L_\kappa = [2\,\mathrm{Im}(\kappa)]^{-1}$ are longer, thereby extending $d_s = w_b/\cos\theta_{sp} + L_\kappa$ (launch site + decay length). Similarly, for the same material Au, SP excitation in the infrared results in much longer L_κ. The overall process amounts to a 230 μm waist (w) asymmetric Gaussian heat source $Q(\bar{r}) \propto \exp[(-|\bar{r}$

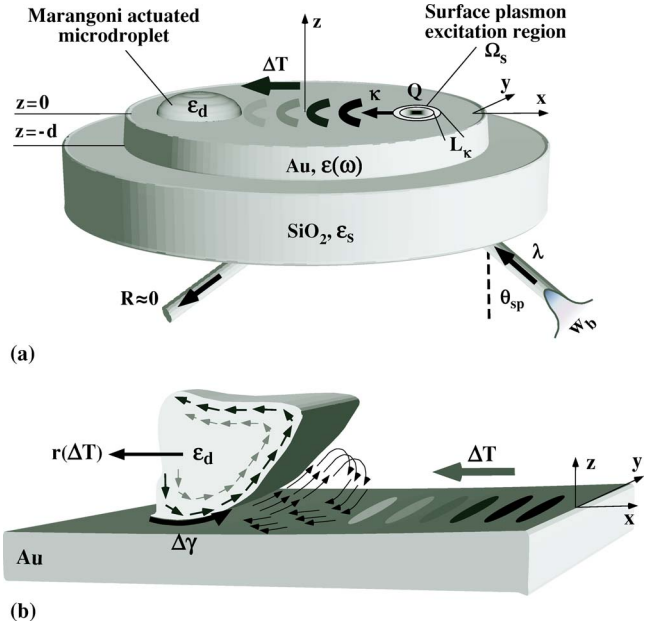

FIG. 1. (Color online) (a) Schematic of the top layer of the Kretschmann configuration including the droplet with the dielectric function ϵ_d. A $d=34$ nm gold film $[\epsilon(\omega)]$ is deposited on a quartz (ϵ_s) 90°-triangular prism (upper part shown only). A thermal gradient of magnitude ΔT is installed as a result of the decay of SPs of wave vector κ, resonance angle θ_{sp}, and decay length L_κ. The xy plane represents the Au-droplet interface. (b) Schematic representation of the solid-liquid interface. The induced surface tension gradient $\Delta\gamma$ gives rise to Marangoni convection actuating the droplet to a new location r. The momentum transfer to the surrounding air molecules establishes a flow that under proper conditions may temporarily prevent coalescence to an approaching droplet.

$-\bar{r_s}|/w)^2]$, where $\bar{r}_s$, denotes the source center coordinates, and $z=0$ defines the liquid-metal interface, such that the total power P delivered is $\int_{-d}^{0}dz\int_{\Omega_s}Q(\vec{r})d^2r$. This energy is transported away from Ω_s primarily by conduction in Au and quartz, and convection to air, due to the low emissivity (<0.01) of Au.

At the metal liquid interface Ω_{ML}, the surface modes are determined by both dielectric functions $\epsilon(\omega)$ and ϵ_d as in $0=[\epsilon(\omega)+\epsilon_d]/2$ for the simpler case of a liquid bounded metal half space. At this interface, for a closest point distance between Ω_{ML} and Ω_s of 30 μm, a thermal gradient of magnitude ΔT is built up within a fraction of a μs, and heat will diffuse into the droplet. The presence of this gradient in the region Ω_{ML} results in sufficient surface tension gradient which derives the Marangoni convection.

We now proceed by experimentally examining the mechanism of sustaining a temperature gradient by the decay of surface plasmon, as elaborated above. We seek to provide qualitative evidence of the thermal effect exhibited by the thin film as a result of the optical excitation of SPs. The metal surface was thus investigated in the absence of the droplet employing a pump-probe technique, shown in Fig. 2. A probe laser, of wavelength 635 nm and output power $P=1$ mW, and a corresponding position sensitive detector (PSD) are aligned in the z direction and navigated systematically in xy directions to scan a region of the gold film, where SPs are excited by a 514 nm line of an Ar^+ laser at an output power of 50 mW. A mechanical chopper intensity-modulated the excitation beam at a frequency of 100 Hz for the objective of generating a satisfactory signal-to-noise ratio, and provided a reference signal for a lock-in amplifier, which monitored the output of the PSD.

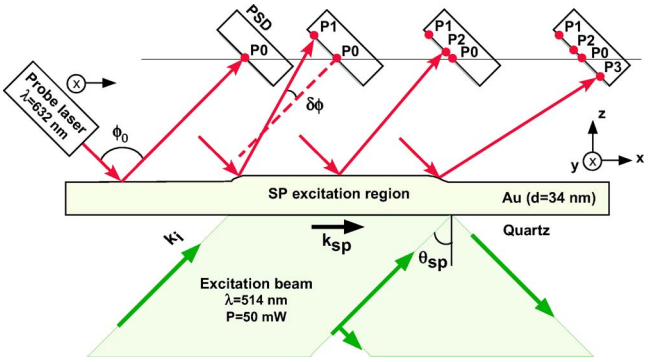

FIG. 2. (Color online) Schematic of the top layer of the Kretschmann configuration in the absence of the droplet and augmented with an optical probing system. A probe laser associated with a position sensitive detector (PSD) is scanned over a region of the gold film, where SPs are excited. This allows for the metallic surface profile to be sensed such that thermal expansion and/or shift in the dielectric function of the system may be quantified. The presence of a temperature gradient may therefore be verified.

Our preliminary measurements reveal that, even at the low excitation laser power used, a striking response is observed, as shown in Fig. 3. The PSD was preliminary configured one dimensionally (detecting beam displacement in one direction only) so that the final beam-deflection image is envisioned to be toroidal (doughnut-shaped). We note that the detected signal is proportional to the extent of the deflection of the reflected probe beam, which appears to be largest at the peripheries of the excitation region, where the "slope"

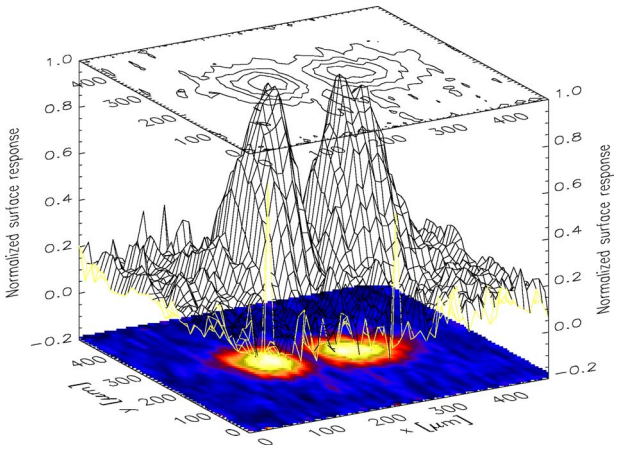

FIG. 3. (Color online) Lock-in detection of the surface modification induced by the decay of surface plasmons. The 750 μm $\times$750 μm scanned area was chosen to be larger than the 300 μm $\times$400 μm cross sectional dimensions of the excitation Ar^+ beam. The observed profile was generated by scanning a uniform mesh of 15 μm cell size, and normalizing the detected signal.

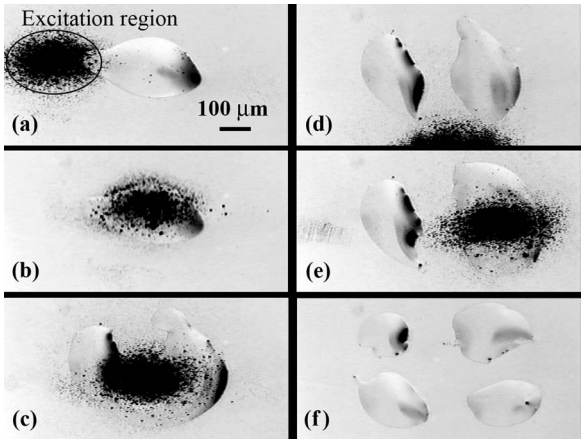

FIG. 4. Transport results when a ΔT is created across Ω_{ML} in primarily one direction. The source power required to create a sufficient ΔT for the transport of the droplets across the surface was measured to be $P=30$ mW for SO, and (due to higher γ and ν) $P=57$ mW in the case of Gl. In the series of pictures (a)–(c), a SO droplet is split first in two, and further into four subdivisions as shown in the images (d)–(f). The color content of the image has been inverted for clarity. ΔT has more than one direction.

is largest. This is schematically depicted in Fig. 2, where the deflection of the reflected probe beam is demonstrated to vary from position $P0$, when sensing the region exterior to the excitation region, to $P1$ at the first measurable encounter with the modified region, to $P2$ at the central part, and finally to $P3$ at the exiting boundary.

Although, the objective of the present work is not to investigate the origin [17] of the observed signal, we note that temperature dependence of the dielectric function of the system is the primary factor at work. Variation in the dielectric function due to volumetric effects such as thermal expansion locally causes a physical deformation of the film's surface, as schematically shown in Fig. 2, whereas variations in the collisional (electrons and phonons) processes, alter the damping. We have recently utilized such surface plasmon induced interactions and reported a coupling scheme that involves multiple photon energies [18,19]. It is also noteworthy to differentiate the measurement of the SP near field effects and decay, in the interior and in the vicinity of the SP launch site, for example such as those provided by a photon scanning tunneling microscope (PSTM) [20,21], and the current thermo-optic effects investigated. We here limit our considerations to the case where we report the observation of a surface plasmon thermal process and verify the presence of a temperature gradient, which we deem accountable for the droplet actuation and exclude any explicit electromagnetic effects such as those occurring during electrophoretic interactions. Figure 3 testifies that a localized thermal gradient does occur at the gold surface.

As the $\Omega_{ML}-\Omega_s$ distance is reduced several events occur. The droplet begins to become disturbed when the edge of Ω_s is approximately 30 μm away in the direction of SP propagation, verifying that a thermal gradient extends beyond the region of plasmon coupling, shown in Fig. 4. We note that the surface plasmon decay length for our working wavelength ($\lambda=514$ nm) and metal [16] ($\epsilon=-3.9+2.7i$) is approximately 0.52 μm. For SO, and Gl in Fig. 4, part of the droplet increases in temperature, decreases in viscosity, reduces surface tension, and recedes from the oncoming thermal gradient. As the laser beam begins to travel underneath the droplet, the SP resonance efficiency drops because the changes in the refractive index over the Au film alters the resonance conditions. Figures 4 and 5 demonstrate in sequences of snapshots the operation of the microfluidic actuation. The versatility of the scanning optical excitation allows for separation of various species by tuning the beam power to a threshold capable of transporting one species only. Figure 5 demonstrates such a differentiation and sorting of the SO and Gl. By positioning Ω_s near a 250 μm SO droplet in a new series of measurements, and turning the SP excitation beam on, the speed of the droplet was measured by post-processing the acquired data. From the analysis of a 30 frames/s digital recording the edge of the droplet receded away from Ω_s at approximately 100 μm/s.

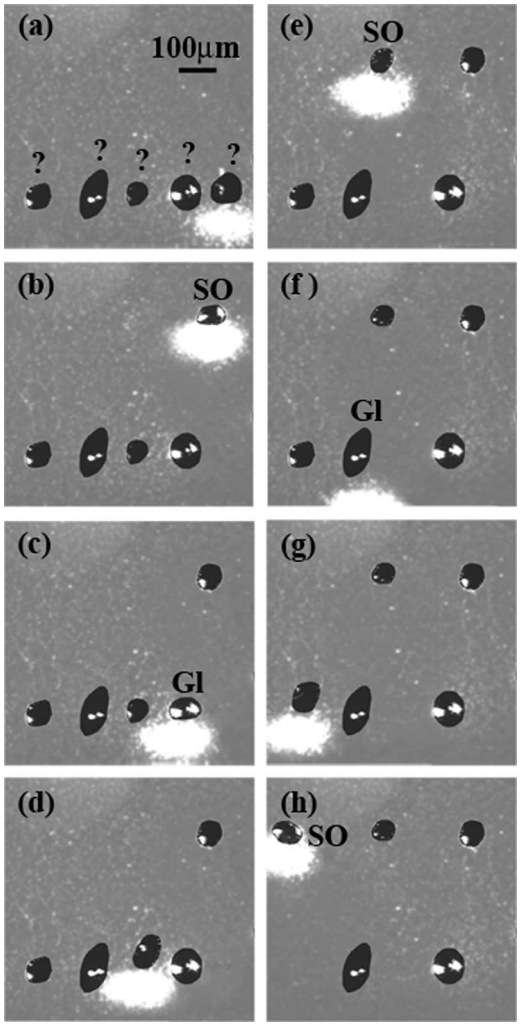

FIG. 5. Liquid ordering by tuning the intensity of the SP excitation. Differentiation and sorting occur when a thermal gradient ΔT of specific magnitude is created, that is only capable to cause one type of analyte to be transported as shown here with SO and Gl droplets. The initial set of unidentified droplets in (a) has been grouped in two sets as shown in (h).

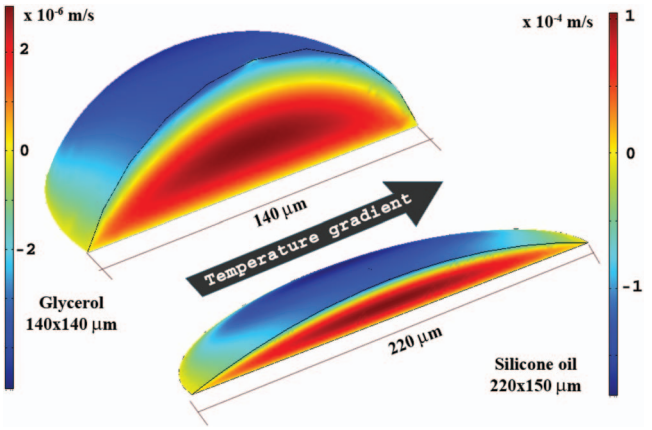

FIG. 6. (Color) Velocity component in the direction of the temperature gradient on the boundary of the computational domain for Gl droplet and SO droplet. The SO droplet having a contact angle of $\theta_c=10°$ wets the surface more than the Gl with a contact angle of $\theta_c=50°$ (see parameters in Table I).

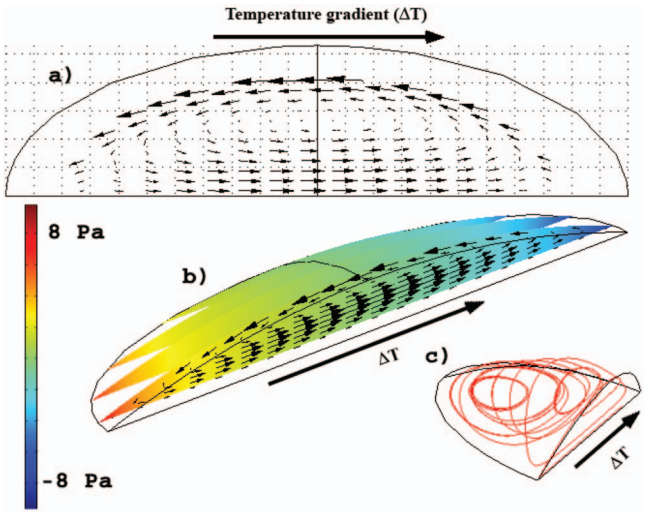

FIG. 7. (Color) Internal structure of the flow inside a droplet of SO. (a) Velocity vectors at a horizontal plane at midheight. (b) Vertical slices with pressure field and velocity vectors at a vertical plane parallel to ΔT and near the symmetry plane. (c) Streamlines inside the droplet.

III. COMPUTATIONAL RESULTS AND DISCUSSIONS

Numerical experiments were conducted in order to investigate the internal flow driven by the Marangoni effects inside the droplets. Though migration and spreading of liquid droplets on solid surfaces may be studied by simplified equations as in lubrication theory [22,23], here we choose the Navier-Stokes equation with the aim that the methodology may be elaborated for treatment of more general cases than those investigated in the current phase of the experiment. The shape of the droplets was taken to be constant, approximated using contact angle measurements. The steady Navier-Stokes equation, $\rho_L \bar{u}\cdot\nabla\bar{u}=\nabla\cdot\tau$ and the continuity equation, $\nabla\cdot\bar{u}=0$, for an incompressible fluid were solved numerically together with the homogeneous energy equation $\rho_L C_L \bar{u}\cdot\nabla T=\nabla\cdot(k_L\nabla T)$. In these equations, ρ_L, k_L, and C_L, denote the density, the thermal conductivity, and the heat capacity of the fluid, respectively, with $\bar{u}$, τ, and T, representing the velocity field, the stress tensor, and the temperature field inside the droplets, respectively. Assuming that the liquid behaves Newtonian, the stress tensor, τ, can be related to the pressure field and the strain rate according to $\tau_{ij}=-p\delta_{ij}+\mu_L(\partial_j u_i+\partial_i u_j)$, where μ_L denotes the dynamic viscosity of the liquid. The above equations subjected to appropriate boundary conditions can be solved numerically using a finite-element technique [24]. For Navier-Stokes, a coupled solver, where all unknown variables are treated simultaneously, is used. Here, it was assumed that the temperature at Ω_{ML} is increasing linearly with x at a given rate. No-slip conditions were applied at this boundary of the droplet. The upper free surface of the droplet was assumed to behave adiabatically, and the force balance relation was written as $t_i\tau_{ij}n_j=-\Gamma_L t_j\partial_j T$, where t_i and n_i denote the i component of the unit vectors tangent and normal to the free surface of the droplet, respectively, and $\Gamma_L=\partial\gamma_L/\partial T$ denotes the variation of the surface tension with temperature. Assuming the free surface of the droplet being adiabatic is justified by the small dimension of the droplet, the above equations and boundary conditions were solved for a 50 μm high Gl droplet with a diameter of 70 μm and a 20 μm high SO droplet being 220 μm long and 150 μm wide. These droplets are subject to a positive temperature gradient of 10°/mm. As expected and presented in Fig. 6, ΔT on the free surface initiates a velocity field, forcing the fluid near the free surface to move from the warm side to the cold side. The resulting maximum velocity is of the order of 100 μm/s in the case of SO and about 100 times lower for Gl, standing in a good agreement with our experimental measurement. The lower speed is simply related to the higher viscosity of Gl in comparison to SO.

Figure 7 details the results of the three dimensional simulation for the case of SO. A complex flow pattern is set up inside the droplet, resulting in a flow in the negative direction of ΔT in regions close to the free surface. The fluid turns after reaching the coldest region of the droplet and moves toward the warm side in the center of the droplet. The negative pressure on the warm side and the positive pressure on the cold side of the droplet signal a change of the shape of the droplet that, in the physical experiments, has led to the rolling mechanism resulting in transport of the droplet. Although the complete nonlinear coupled set of equations for conservation of mass, momentum, and energy was considered here, the results show that nonlinearities are relatively small, and the deviations in the temperature field from the values set on Ω_{ML} are negligible. Consequently, the results can be rescaled safely for other values of temperature gradient within reasonable limits.

IV. CONCLUSION

In conclusion, we have investigated the surface modes of a droplet and a thin metal film to demonstrate the physical manipulation of microdroplets by optical means. Excitation and modulation of SPs for the particular purpose presented here define a border line between optics and microfluidics,

with the potential of opening up several possibilities. Owing to the high thermal conductivity of Au, and short life time of SPs, dynamic effects, such as droplet oscillations, can be studied by modulated SP excitation on time scales as short as microseconds depending on, among others, inertial properties of the droplet. This, in combination with local field enhancement of SPs, can open up new opportunities. The Kretschmann system may be augmented with a low power laser beam dedicated to SPR sensing only. As the actuating beam (Marangoni) navigates the microdroplets, the sensing beam probes the variations in the dielectric function as the droplet arrives. A potential application here may also include obtaining physical properties of liquids. Auxiliary beams that operate from above the droplet, such as the probe beam discussed, may be added allowing for monitoring the conditions of the open surface of the droplet. SP spectral capabilities and phenomena such as SP interference [21] may provide further control in fluid confinement in nanometer regions. Determination of dependence of the discussed fluidic operations upon the droplet size remains to be assessed. However, for the same temperature gradient prevailing on the metal surface, it is conceivable that a lower size-limit may exist such that smaller droplets may not sense the gradient and thus locally experience a uniform temperature disabling their motion.

ACKNOWLEDGMENTS

This work was supported by the DOE Office of Biological and Environmental Research. Oak Ridge National Laboratory, Oak Ridge, Tennessee, 37831-6123, is managed by UT-Battelle, LLC for the Department of Energy under Contract Number DE-AC05-0096OR22725.

[1] N. H. March and M. P. Tosi, *Liquid State Physics* (World Scientific, Singapore, 2002).
[2] L. E. Scriven and C. V. Sternling, Nature (London) **187**, 186 (1960).
[3] J. Thomson, Philos. Mag. **10**, 330 (1855).
[4] H. Bénard, Rev. Gen. Sci. Pures Appl. **11**, 1261 (1900).
[5] P. Dell'Aversana and G. P. Neitzel, Phys. Today **51**, 38 (1998).
[6] R. H. Ritchie, Phys. Rev. **106**, 874 (1957).
[7] H. Raether, *Surface Plasmons on Smooth and Rough Surfaces and on Gratings*, Springer Tracts in Modern Physics (Springer-Verlag, Berlin, 1988).
[8] C. G. M. Marangoni, Ann. Phys. Chem. **143**, 337 (1871).
[9] A. A. Darhuber and S. M. Troian, Annu. Rev. Fluid Mech. **37**, 425 (2005).
[10] R. H. Farahi, A. Passian, T. L. Ferrell, and T. Thundat, Appl. Phys. Lett. **85**, 4237 (2004).
[11] G. L. Liu, J. Kim, Y. Lu, and L. P. Lee, Nat. Mater. **5**, 27 (2005).
[12] R. H. Farahi, A. Passian, T. L. Ferrell, and T. Thundat, Opt. Lett. **30**, 616 (2005).
[13] The study of pure Marangoni contribution is an ongoing research carried out under microgravity environment of space programs, where buoyancy convection tend to zero.
[14] SO is nontoxic, transparent with stable (T dependent) γ for contamination, is the fluid of choice in the context of this work. Gl with its higher γ was chosen for the sorting experiment.
[15] E. Kretschmann, Zeitschrift für Physik **241**, 313 (1971).
[16] E. D. Palik, *Handbook of Optical Constants of Solids* (Academic Press, New York, 1985).
[17] A. L. Lereu, A. Passian, R. H. Farahi, T. L. Ferrell, and T. Thundat (unpublished).
[18] A. Passian, A. L. Lereu, E. T. Arakawa, A. Wig, T. Thundat, and T. L. Ferrell, Opt. Lett. **30**, 41 (2005).
[19] A. Passian, A. L. Lereu, R. H. Ritchie, F. Meriaudeau, T. Thundat, and T. L. Ferrell, Thin Solid Films **497**, 315 (2006).
[20] P. M. Adam, L. Salomon, F. de Fornel, and J.-P. Goudonnet, Phys. Rev. B **48**, 2680 (1993).
[21] A. Passian, A. L. Lereu, A. Wig, F. Meriaudeau, T. Thundat, and T. L. Ferrell, Phys. Rev. B **71**, 165418 (2005).
[22] P. Erhard and S. H. Davis, J. Fluid Mech. **229**, 365 (1991).
[23] M. K. Smith, J. Fluid Mech. **294**, 209 (1995).
[24] Femlab 3.0 (http://www.comsol.com/)is a general finite-element code used for solving partial differential equations.